

Metal–Organic Frameworks and Their Hybrid Composites for Adsorption of Volatile Organic Compounds

Shella Permatasari Santoso^{1,2*}, Artik Elisa Angkawijaya³, Vania Bundjaja¹,
Felycia Edi Soetaredjo^{1,2} and Suryadi Ismadji^{1,2}

¹*Chemical Engineering Department, Widya Mandala Surabaya Catholic University, Surabaya, East Java, Indonesia*

²*Department of Chemical Engineering, National Taiwan University of Science and Technology, Taiwan, Taipei*

³*Graduate Institute of Science and Technology, National Taiwan University of Science and Technology, Taiwan, Taipei*

Abstract

Environmental pollution caused by anthropogenic emissions is a growing concern throughout the world; volatile organic compounds (VOCs) are the main constituents that make up the emissions. In handling VOCs, adsorption is considered the most efficient method to date. Engineers have been intensively studied the synthesis and usage of metal–organic frameworks (MOF) as versatile adsorbents for many types of VOC. Improving adsorption efficiency and performance is a routine agenda in the development of the MOF; prior to achieving an efficient MOFs as VOCs adsorbents, insight to MOF-key features such as structure, pore, and the functional group is very crucial. To this end, several topics related to adsorption of VOCs by MOF is discussed; specifically, the adsorption performance of some MOFs against VOCs, the effect of some key-features of MOF to the adsorption performance, the development of MOF composite for improvement of adsorption performance, analytical method for modeling the adsorption, and factors influencing the adsorption performance.

Keywords: Metal–organic framework, MOF, volatile organic compound, adsorption, porous adsorbent, dynamic sorption, breakthrough curve

*Corresponding author: shella_p5@yahoo.com

12.1 Introduction

The deployment of air pollution caused by toxic and hazardous substances worsens as a result of the rapid increase in anthropogenic emissions. Chemicals combustion, evaporation, reaction, and purification are the predominant sources of anthropogenic emissions and are growing concerns of worldwide. A substantial amount of hazardous gases such as hydrocarbons, volatile organic compounds, sulfuric compounds, nitrogen compounds, and greenhouse compounds are produced from those emissions. The volatile organic compounds (VOCs) are considered as major air pollutants since they always produced in every activity involving chemicals [1, 2]. As reported by the United States Environmental Protection Agency (US EPA), 50% of VOCs is contained in the emission of fossil fuel combustion [3]. Moreover, given the continuous development of industry throughout the world, it is prominent that VOCs emissions will continue to increase in the future.

VOCs are those organic compounds that quickly evaporate at standard ambient conditions. Acetone, benzene, chloroform, ethanol, formaldehyde, isopropanol, naphthalene, propane, and toluene are several types of VOCs. VOCs are dangerous health threats that are often underestimated since they are commonly not physically visible. The entry of VOCs into the respiratory tract leads to various health problems ranging from mild to acute, such as irritation, headache, nausea, tissue or organ damage, and cancer. Unwittingly, VOCs pollutions may come from daily items and/or various surrounding materials; i.e., natural gas, paint, adhesive, candle, room freshener, ink, household cleaner, cigarette, varnish, disinfectant, rubbing alcohol, pesticide, cosmetic, etc. VOCs have a peculiar strong odor that signifies high concentration, at low concentration the odor may remain unnoticeable; nevertheless, the damaging effects may potentially fatal. The presence of VOCs as an airborne contaminant can aggravate global warming since they cause stratospheric depletion, greenhouse effect, and smog accumulation. Thus VOCs considered as one of the root of climate problems [1–4].

Numerous VOCs removal techniques have been introduced, including photo-catalysis, filtration, oxidation, biological degradation, condensation, and adsorption [5, 6]. Adsorption by using natural or synthetic adsorbent is the most frequently performed since it offers various advantages such as flexible (can be used in removal of specific or non-specific VOCs), low cost, simple, and controllable. The development of engineered-adsorbents has been substantially examined with priority to acquire adsorbent that effectively eliminates VOCs. Out of various engineered-adsorbents,

metal-organic frameworks (MOFs) are being intensively developed as adsorbent of VOCs; MOFs offer a large specific surface area that relates to the adsorption ability. MOFs can be easily constructed, designed, and fabricated by coordinating organic compound (ligand) and metal at the particular condition. Some MOFs possess semiconducting nature that makes them capable of self-regeneration by photo-degrading the VOCs. Furthermore, recyclability is also one of the superiority of MOFs. Provided with those superior properties, the emergence of utilization and development of MOFs to eliminate VOCs is obviously visible.

12.2 VOCs and Their Potential Hazards

VOC is an epithet for carbon-containing compounds, which possess distinct characteristics such as high vapor pressure, low boiling point, evaporate freely, and reactive at a standard temperature and pressure. There are certain usual extents, related to the characteristics of VOCs, between each country that causes a slight difference in the definition of VOCs. Several agencies issuing the standard of VOCs are National Institute for Occupational Safety and Health (NIOSH), Environmental Protection Agency (EPA), Air Quality Management (AQM), Environmental Protection Department (EPD), Department of Occupational Safety and Health (DOSH), etc. In general, the standards over the countries gives the following specific characteristics of VOCs; *viz.* boiling point of 50°C to 250°C and vapor pressure equal to 0.01 kPa (9.87×10^{-5} atm) or higher (measured at 293.15 K and 101.325 kPa). VOCs sources increase every decade due to increasingly diverse type of emissions that may come both from natural sources and anthropogenic sources. Undoubtedly anthropogenic sources, which mainly due to the rapid development of industrial sections in various parts of the world, contribute the highest VOCs emissions. Daily activities such as cooking, smoking, driving, printing, and burning, are also pay a role for this VOCs emissions [3, 7].

VOCs come in a variety of structures ranging from aromatic, alcohol, aldehyde, alkene, ketone, polycyclic, and halogenated forms, as listed in Table 12.1. The concentration index of VOCs that is likely to cause dangerous threat is proposed by NIOSH as immediately dangerous to life and health (IDLH). The index can be expressed as recommended exposure limit (REL) from adverse health effects over a working lifetime, and 10% of the lower explosive limit (LEL) for safety considerations related to the potential for explosion hazards. Health and/or life threats caused by VOCs vary depending on the length of exposure time, number of toxicants, and

Table 12.1 Properties of some VOCs and their IDLH levels as proposed by NIOSH [8].

Compound	Formula	b.p. (K)	p (kPa)	IDLH	
				REL (mg/m ³)	LEL (ppm)
Alcohols					
Ethyl alcohol	C ₂ H ₅ OH	351.39	7.91	1,900 ^b	3,300
Methyl alcohol	CH ₃ OH	337.85	16.93	260 ^b	6,000
Isopropyl alcohol	CH ₃ CHOHCH ₃	355.45	6.05	980 ^b	2,000
Phenol	C ₆ H ₅ OH	454.90	0.05	19 ^a	1,800
Aldehydes					
Acetaldehyde	CH ₃ CHO	293.95	120.26	n.e.	4,000
Formaldehyde	H ₂ CO	253.65	518.62	n.e.	7,000
Benzaldehyde	C ₆ H ₅ CHO	451.85	0.17	NA	1,400
Alkanes					
n-Hexane	C ₆ H ₁₄	341.88	20.40	180 ^a	1,100
n-Heptane	C ₇ H ₁₆	371.53	6.13	350 ^a	1,050
Octane	C ₈ H ₁₈	398.77	1.88	350 ^a	1,000

(Continued)

Table 12.1 Properties of some VOCs and their IDLH levels as proposed by NIOSH [8]. (Continued)

Compound	Formula	b.p. (K)	p (kPa)	IDLH	
				REL (mg/m ³)	LEL (ppm)
Aromatics					
Aniline	C ₆ H ₅ NH ₂	457.25	0.09	n.e.	1,300
Benzene	C ₆ H ₆	353.23	12.64	3.2 ^a	1,200
Toluene	C ₇ H ₈	383.75	3.79	375 ^a	1,100
Naphthalene	C ₁₀ H ₈	491.05	0.01	50 ^a	900
Chlorobenzene	C ₆ H ₅ Cl	404.75	1.60	NA	1,300
Carboxylics					
Acetic acid	CH ₃ COOH	391.05	2.09	25 ^a	4,000
Formic acid	HCOOH	374.15	5.68	9 ^a	18,000
Esters					
Ethyl acetate	CH ₃ COOC ₂ H ₅	350.25	12.43	1,400 ^a	2,000
Diethyl phthalate	C ₆ H ₄ (COOC ₂ H ₅) ₂	568.15	0.0003	5 ^a	700*
Halogenated					
Benzyl chloride	C ₆ H ₅ CH ₂ Cl	447.15	0.16	5 ^c	1,100

(Continued)

Table 12.1 Properties of some VOCs and their IDLH levels as proposed by NIOSH [8]. (Continued)

Compound	Formula	b.p. (K)	p (kPa)	IDLH	
				REL (mg/m ³)	LEL (ppm)
Chlorine	Cl ₂	239.11	777.27	1.45 ^c	n.f.
Chloroform	CHCl ₃	334.27	26.26	9.78 ^b	n.f.
Ketones					
Acetone	(CH ₃) ₂ CO	329.23	30.80	590 ^a	2,500
2-Butanone	CH ₃ C(O)CH ₂ CH ₃	352.74	12.08	590 ^a	1,400
Cyclohexanone	(CH ₂) ₅ CO	428.75	0.67	100 ^a	1,100
Peroxides					
Hydrogen peroxide	H ₂ O ₂	423.35	0.26	1.4 ^a	n.f.
Pnictogens					
Ammonia	NH ₃	239.80	999.92	18 ^a	15,000
Dimethylamine	(CH ₃) ₂ NH	280.45	202.65	18 ^a	2,800
Miscellaneous					
Hydrogen sulfide	H ₂ S	212.82	2026.50	15 ^a	4,000

n.e. none established (potential occupational carcinogenic); n.f. nonflammable; n.a. not available.

^a8-h time-weighted average (TWA); ^b60-min short-term exposure limit (STEL); ^cCeiling value

*measured at 368°F = 459.8 K

route of exposure. Age and pre-existing health conditions are also determining factor in level of hazard.

Acute health effect usually can be seen soon after exposure includes irritation to the eyes, skin, upper respiratory—the nose, nasal cavity, and throat, and lower respiratory—the larynx, trachea, bronchi, and lungs, and other short-term effects such as headache, grogginess, drowsiness, fatigue, nausea, and vomiting. Long-term exposure of some VOCs is associated with persistent diseases and even life-threatening diseases, such as damage of liver, kidneys, lungs, nerves, and other organs [8]. Known and probable human carcinogenic properties were also observed for several VOCs as reported by the International Agency for Research on Cancer (IARC) and the US National Toxicology Program (NTP). Health and/or life threats caused by VOCs vary depending on their reactivity.

12.2.1 Other Sources of VOCs

Air emissions by VOCs are traditionally only associated with various anthropogenic activities. However recent observations revealed that biomass also contributed to the VOCs emission. The VOCs emitted by biomass is known as biogenic volatile organic compounds (*bVOCs*); with isoprene, methanol, acetone, acetaldehyde, limonene, and myrcene are several types of *bVOCs*. Soil is commonly linked to the emission of *bVOCs* due to biotic or abiotic activities of living organisms in soil. *bVOCs* produced by the living organisms mostly end up buried and accumulated in the soil; then, after certain (high) concentration, the *bVOCs* are released from soil. In this context, soil may acts as a complex-adsorbent material that restrains the immediate release of *bVOCs* [9].

The litter of diverse pine trees can produce *bVOCs* including acetone, methanol, acetaldehyde, ethane, hexane, also some groups of alkanes, and terpenes. The emission rates of those *bVOCs* are relatively low, between 936 to 0.35 $\mu\text{g}/\text{m}^2$ in an hour. This emission rate normally increased at hot season due to increased temperature and solar irradiance. Some studies revealed that plant-roots commonly emit *bVOCs* in the form of aldehydes, alcohols, and ketones [9, 10]. Microorganisms, such as bacteria and fungi, dwell in the soil also contributed to the formation of *bVOCs* as a result of their metabolism. *Bacillus subtilis* metabolism is known to produce 2,3-butanediol. *Saccharomyces cerevisiae* and *Lactobacillus* produce ethanol in their fermentation. *Clostridium* species fermentation produces acetone and butanol. Biodegradation of organic matter done by microorganisms is known to produce methane, one of the greenhouse gases.

Some flavoring compounds, such as pyrazines, are produced from the biosynthesis of some bacteria. A similar type of *b*VOCs can also be produced by fungi [9, 10].

Although *b*VOCs are usually not being considered as hazardous substances due to their relatively low emission rate and their natural characteristics, it is worth to mention to broaden insight about VOCs sources. Moreover, some *b*VOCs are known to have antifungi activity and plant-growth promoting effect. For instance, bacteria-VOCs can inhibit the growth of phytopathogenic fungi *Rhizoctonia solani*. Trimethylamine, dimethyloctylamine, and benzaldehyde produced by bacteria are known to have strong antifungi activity. Ryu *et al.* stated that 2,3-butanediol produced by bacteria could promote the growth of plant [11]. Several other *b*VOCs and their producing organism are listed in Table 12.2.

12.3 VOCs Removal Techniques

A considerable number of VOCs handling techniques are mandatory due to the noticeable harmful impact of VOCs on environmental sustainability and human health. There are two fashions in the handling of VOCs that is recovery-based and destruction-based techniques [6]. Recovery technique is based on the idea of capturing VOCs using a transfer media to be reused later; the method is including adsorption, evaporation–condensation, absorption, and membrane separation. Whilst, destruction technique is a process of degrading VOCs into air constituents such as water vapor and carbon dioxide by combustion, oxidation, biodegradation, or plasma treatment [6]. Some studied removal techniques of VOCs are listed in Table 12.3. So far, recovery-based methods are more appealing than destruction-based methods from many viewpoints such as:

- VOCs recovery allow for reuse which is considered beneficial economically
- Absence of environmentally toxic by products such as reactive oxygen species and greenhouse gases
- Low energy necessity
- Comparable removal efficiency with the destruction techniques
- A relatively shorter process

Table 12.2 Some biogenic volatile organic compounds and their producing organisms.

Biomass	Produced VOCs	Ref.
Plant species		
<i>Arabidopsis thaliana</i> (mouse-ear cress)	Limonene, ethyl acetate, rhizathalene, ethanol, aldehydes, ketones	[12]
<i>Artemisia tridentate</i> (sage brush)	Limonene, nerol, camphor, caryophyllene, neryl isovalerate	[13]
<i>Citrus aurantium</i> (bitter orange)	Monoterpenes (e.g, limonene, terpinolene, sabinene, camphene, camphor, carvone, geranyl acetate), monoterpeneoid (e.g, linalool, citronellol, geraniol, nerol, citronellal, perillaldehyde), 1-octanol, octanal, dodecanal, decanal	[14]
<i>Pinus sylvestris</i> (Scots pine)	Acetone, isoprene, tricyclene, α - and β -pinene, camphene, limonene, careen, γ -lirpinene	[15]
<i>Zea mays</i> (corn)	Hexadecanal, tetradecanal, β -macrocarpene, β -bisabolene, (<i>E</i>)- β -caryophyllene	[16]
Bacteria species		
<i>Saccharomyces cerevisiae</i>	Ethanol, ethyl acetate, 3-methyl-1-butanol, 2-methyl-1-butanol, ethyl octanoate, phenylethyl alcohol	[17]

(Continued)

Table 12.2 Some biogenic volatile organic compounds and their producing organisms. (Continued)

Biomass	Produced VOCs	Ref.
<i>Wickerhamomyces anomalous</i>	Acetaldehyde, ethyl acetate, ethyl butyrate, isoamyl acetate, ethyl hexanoate, phenylethyl acetate 2-phenyl-ethanol, isobutanol, amylic alcohol, isoamyl alcohol	[18]
<i>Lactobacillus helveticus</i>	Ketones (e.g., 2-propanone, 2-butanone, diacetyl), esters (e.g., ethyl acetate, ethyl butanoate, isoamyl acetate), benzaldehyde, phenylacetaldehyde, phenylethanol, ethanol, 2- and 3-menthylbutanal	[19]
<i>Staphylococcus aureus</i>	3-Methyl-butanal, 3-methyl-butanoic acid	[20]
<i>Clostridium beijerinckii</i>	acetone, butanol, ethanol	[21]
Fungi species		
<i>Muscodor vitigenus</i>	Naphtalene	[22]
<i>Phomopsis</i> sp.	Sabinene, 1-butanol, 3-methyl, benzeneethanol, 1-propanol, 2-propanone	[23]
<i>Phoma</i> sp.	Trans-caryophyllene, naphthalenes, alcohols	[24]
<i>Trametes versicolor</i>	δ -cadinene, β -guaiene, γ -patchoulene, isolekene	[25]
<i>Metarhizium anisopliae</i>	<i>n</i> -tetradecane, alkenes	[26]

Table 12.3 Several studied VOCs removal techniques and their performance.

Technique	Material	VOC	Operating condition	Removal efficiency	Ref
Destruction-based techniques					
Catalytic oxidation	Au/MnO _x /3DOM SiO ₂	Toluene	225°C	90%	[31]
Thermal oxidation	Porous cordierite packed bed	Mix: methanol, xylene, ethyl acetate	400–975°C	90%	[32]
Biofiltration	<i>Candida utilis</i> biofilm on sugar cane bagasse	Ethanol	30°C, pH 6, moisture 63%	70%	[33]
Recovery-based techniques					
Absorption	Polypropylene bioscrubber	Mix: oxygenated, aromatic, halogenated	Room temp.	12–36%	[34]
Adsorption	Diatomite stellerite vitric tuff	butyl propionate	25°C	9.2% 59.3% 20.5%	[30]
Membrane separation	Poly-dimethyl-siloxane/ α -alumina membrane	Mix: toluene, propylene, butadiene	21°C, 3–5 mbar	95%	[35]

Adsorption is acknowledged as the most favorable recovery-based VOCs elimination techniques because of its notable effectiveness (selective for each type of adsorbent and adsorbate), practical operation, and economic feasibility [27–30]. The characteristic of the solid adsorbent (porosity, selectivity, and activity) play the most vital role in the performance of adsorption. Metal organic framework (MOF) is a rising adsorbent material that is recognized for its large surface area, high porosity, ease fabrication, modifiable selectivity, high efficiency, etc. Many engineering processes are being developed to synthesize MOF with high efficiency in adsorption. The specificity of MOFs for adsorption of certain VOC is very dependent on their active adsorption sites. Many studies stated that high porosity and surface area of MOFs is not adequate for achieving efficient adsorption towards specific VOC gases/vapors. In fact, the strong interaction between host adsorbent and guest adsorbate is depended on each other compatibility. For instance, some interactions (i.e., van der Waals interactions, π – π interaction, and coordination bond) can increase the adsorption efficiency and/or selectivity when unsaturated (open sites) metal centers and organic ligand with certain functional groups interact.

12.4 Fabricated MOF for VOC Removal

Beside the potential of VOCs adsorption, the development of novel MOFs has been extensively carried out in the basis of their extent of freedom and easiness in fabrication, pore tunability, and strong durability. MOFs are constructed from the coordination of organic compounds as the primary building blocks to metal cluster (or ion) as the secondary building blocks. Substantial choices of building blocks are available to synthesize MOFs which offers distinct structural diversity of MOFs. However, a proper understanding of the occurring coordination/interaction between MOF and VOC is crucial prior to gain insight in their adsorption mechanism.

Physically, the adsorption potential of MOFs arises from the porous nature that grants them with large surface area and deep pore volume. The large surface area of MOFs provides large active adsorption sites, while the deep pore volume allows the adsorbate to be entrapped in the pore of MOFs. The choice of building blocks is important in designing the molecular structure of MOFs; it is usually based on the size and chemical features of the building blocks. However, along with progress, more and more cases disclose that the merit of MOFs is not enough for efficient adsorptive removal of VOCs. Instead, effective adsorption requires specific interactions and coordination between the VOCs adsorbate and MOFs adsorbent.

In this section, the adsorption performance of several analogs of MOF, such as MIL series MOFs, the isorecticular MOFs, and some MOF derivatives, is gathered. Only dynamic adsorption of some common VOCs such as acet-aldehyde, acetone, benzene, ethyl acetate, formaldehyde, etc, is discussed.

12.4.1 MIL Series MOFs

MIL, which represents Materials of the Institute Lavoisier, series of MOFs consist of MIL-53, MIL-47, MIL-100, and MIL-101. MIL-53 and MIL-47 share the same geometrical structure, while MIL-100 shares the same structure with MIL-101. The difference in MIL-53 and MIL-47 is mostly based on their properties which caused by the different metal used for the synthesis. In the synthesis of MIL-100 and MIL-101 different type of organic linker (ligand) is used, that is trimesic acid for MIL-100 and terephthalic acid for MIL-101. The building blocks and the shape of MIL series MOFs are presented in Figure 12.1. Here we can see only several metals that often used for the MIL synthesis is given.

MIL-53 consists of three structural analogues that were synthesized with different metal ions, namely Cr, Sc, Fe, or Al, through a hydrothermal reaction between metal nitrate salt and terephthalic acid (H_2BDC) in water (1:0.5:80 in molar ratio) at a temperature of $180^\circ C$. MIL-53 arranged of one

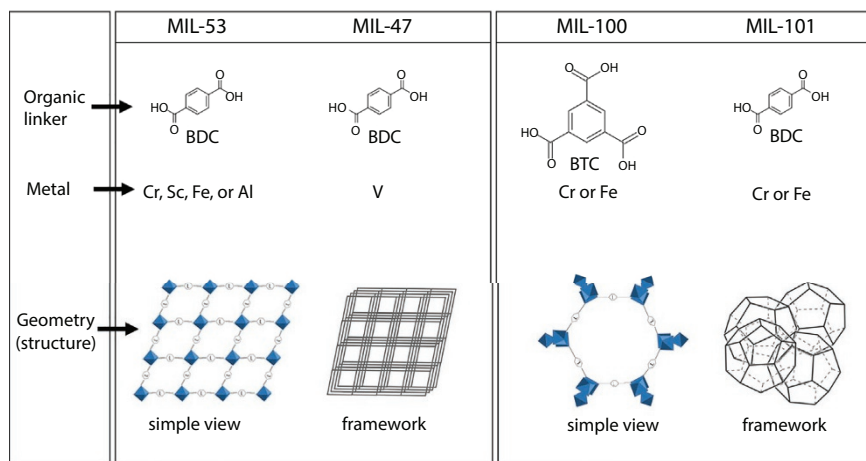


Figure 12.1 Organic and metal building blocks of MIL-53, MIL-47, MIL-100, and MIL-101, and their structures. MIL-53 and MIL-47 built from octahedral metal cluster coordinated to organic linkers to form a 3D network with 1D diamond-shaped pores. MIL-100 and MIL-101 built from trimer of metal octahedral coordinated with organic linkers to form a 3D dodecahedron with the large pore. Adapted from Ref. [36–42].

dimensional parallel chains of the octahedral metal cluster (that is $M(O_4)(OH)_2$, where $M = Cr^{3+}, Fe^{3+}, Sc^{3+},$ or Al^{3+}) coordinated to terephthalic organic linkers into a three dimensional network with diamond-shaped pores (up to 8.5 Å in size) [43–45]. MIL-53 is known to have unique behavior, namely breathing behavior which portrays MIL-53 reversible structural change from an open pore to a closed pore structure. The structural transformation of MIL-53 is induced by heating. An exposure of MIL-53 to high temperature caused pore opening and change in crystalline structure into the orthorhombic crystal system, while low temperature condition caused pore closing and monoclinic crystal arrangement [38, 43–45]. Breathing behavior is explained further in subsection 12.8.1.

Constructed from the same organic linker as the MIL-53, MIL-47 possesses a similar geometry with MIL-53. MIL-47 is constructed with VO_6 octahedral metal cluster, it has a one dimensional pores which shaped like diamond and diameter of 7.5 Å. MIL-47 is as stable as MIL-53, where no structural collapse observed after the adsorption process. MIL-47 has a rigid structure which not allowing the occurrence of breathing behavior. The rigidity of MIL-47 can be preserved up to mechanical pressure of 178.1 MPa; which also confirmed by the X-ray diffraction (XRD). The XRD analysis shows no (or slight) orthorhombic pattern change upon exposure to a pressure up to 178.1 MPa; where the unit cell volume maintained approximately 1500 Å³. At 178.1 MPa, the coexistence of open and closed pores is observed and the crystallinity pattern altered to monoclinic; where the observed unit cell volume (belong to the dominantly closed pore) is 950 Å³ approximately. Further increase in pressure (up to 340.1 MPa) caused the absence of opening pore; the observed unit cell volume is 870 Å³. The pore closing phenomena encountered by MIL-47 does not cause destruction to the framework. The pore can be expanded back upon pressure release (decompression) [38, 42].

MIL-100 build from trimesic acid (H_3BTC) as the organic linker and trivalent metal such as Fe, Cu, Al, or Cr, in common. MIL-100 can be synthesized by hydrothermally reacting the organic compound and metal salt of choice in a water solvent, at the temperature of 200–220°C for 4–8 h. MIL-100 is categorized as a large member of MOFs that have pore size up to 34 Å [37]. MIL-101 can be hydrothermally synthesized from terephthalic acid with metal such as Fe, Cu, Al, or Cr, in common. The reacting condition is similar to that of the synthesis of MIL-100. Earlier synthesis of MIL-101 (also MIL-100) was done by using hydrofluoric acid as solvent, but recent studies showed that either MOF-100 or MOF-101 can be obtained by using water as solvent without addition of hydrofluoric acid [36, 40].

The summarized adsorption capacity of MIL series MOF is available in Table 12.4. Among the MIL series of MOFs, MIL-53(Al or Cr) and MIL-47(V) are the one known to possess reversible adsorption behavior owing to their breathing capability. The reversible properties of MIL-53 and MIL-47 have been extensively studied against hydrogen sulfide (H_2S) gas under different pressure. While the pore structure of MIL-47 remains the same after H_2S adsorption at a pressure below 1.8 MPa; MIL-53 encounter a sequence of pore opening and closing. At high pressure of H_2S , MIL-53 encounters pore opening while at low pressure of H_2S MIL-53 encounters pore closing. Both MIL-53 and MIL-47, are able to maintain their structural stability after the adsorption process. The adsorption in MIL-53 and MIL-47 happened through the H-bonding between the adsorbate and carboxylic groups of the MOFs. In the case of MIL-53, especially with Cr building block, H_2S acts as the H-acceptor. On the contrary, H_2S acts as H-donor against MIL-47(V) [38].

In the similar adsorption process against H_2S as adsorbate, MIL-100(Cr) and MIL-101(Cr) exhibit irreversible desorption due to the partial structural collapse of the building blocks which initiated by the strong adsorptive interactions between H_2S and the MOFs. This phenomenon also indicated the lack regenerative ability of MIL-100 and MIL-101, thus limit its reusability and practical application [38]. The adsorption performance of breathable MOFs (MIL-100 and MIL-101) against other VOCs also has been investigated in other studies. They show different adsorption capacity for each studied VOC. It is emphasized that different type of VOC has a different affinity towards the adsorbent, depending on their dominant bonding characteristics (such as π or σ bond, proton, or H bond, etc.).

12.4.2 Isoreticular MOFs

Isoreticular is a term given for MOFs with similar topological structure. In this section, the dynamic adsorption capacities of six isoreticular MOFs (Figure 12.2), namely, MOF-177, MOF-5, MOF-74, IRMOF-3, MOF-199, IRMOF-62, are discussed. MOF-177 has been widely synthesized and used for the adsorption of gas and VOCs [29, 46–49]. A MOF-177 was synthesized from zinc nitrate hexahydrate as the metal source and synthesized-organic-ligand namely 4,4',4''-benzene-1,3,5-triyl-trisbenzoic acid (H_3BTB) and are used for the preparation of. H_3BTB is a well-known building block for producing MOFs with a high surface area up to 5000 m^2/g ; this property also serves it as a good gas storage material. As previously introduced by many researchers, the

Table 12.4 Studied adsorption performance of MIL series MOFs against some VOCs.

MOF	BET (m ² /g)	Pore volume (cm ³ /g)	Adsorption type	Adsorption model	Adsorption capacity	Ref
MIL-47(V)	~1000	–	Static	–	14.6 mmol/g (H ₂ S).	[38]
MIL-53(Cr)	~1000	–	Static	–	13.12 mmol/g (H ₂ S).	[38]
MIL-53(Fe)	~1000	–	Static	–	11.77 mmol/g (H ₂ S).	[38]
MIL-53(Al)	~1000	–	Static	–	8.53 mmol/g (H ₂ S).	[38]
MIL-100(Cr)	1695	–	Static	SL	0.38 (phenol), 0.20 (<i>p</i> -nitrophenol). Value in mmol/g.	[27]
MIL-100(Cr)	1900	–	Static	–	16.7 mmol/g (H ₂ S).	[38]
MIL-100(Fe)	1675	–	Static	SL	0.38 (phenol), 0.23 (<i>p</i> -nitrophenol). Value in mmol/g.	[27]
MIL-101(Cr)	4293	2.43	Dynamic	FL-PFO	83.44 (benzene), 97.74 (toluene), 7.34 (xylene), 98.47 (<i>n</i> -hexane), 81.97 (<i>n</i> -heptane). Value in wt%.	[41]
MIL-101(Cr)	2736	1.50	Static	DA	0.16 (<i>n</i> -hexane), 0.53 (toluene), 0.83 (butanone), 0.99 (dichloromethane), 1.47 (methanol), 12.8 (<i>n</i> -butylamine). Value of limiting adsorption capacity in mmol/g.	[39]
MIL-101(Cr)	2600	–	Static	–	38.4 mmol/g (H ₂ S).	[38]

FL-PFO: fractal-like pseudo-first-order, DA: Dubinin–Astakhov, SL: Sips and Langmuir.

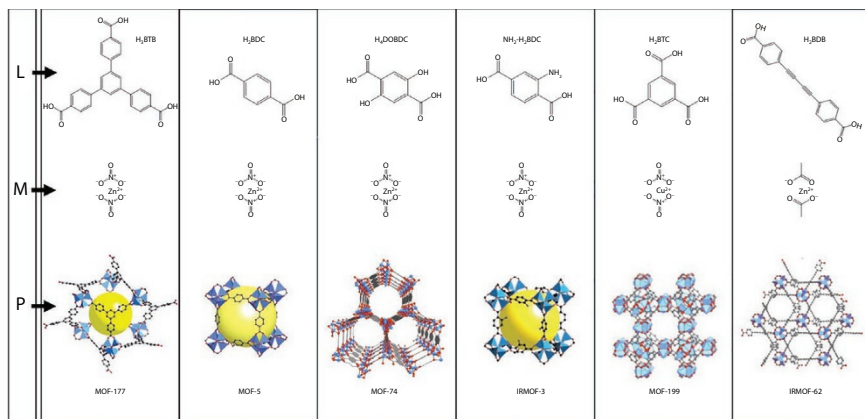


Figure 12.2 Organic and metal building blocks of the isorecticulars MOF-177, MOF-5, MOF-74, IRMOF-3, MOF-199, and IRMOF-62. L = organic ligand, M = metal ion source, and P = MOF product. Adapted from Ref. [46].

preparation of the H_3BTB ligand involve two step reactions; first step by electrophilic reaction involving $AlCl_3$, and second step by Hofmann rearrangement involving $NaOBr$. The preparation of MOF-177 itself is conducted solvothermally, in *N,N*-diethylformamide solvent (common solvent for synthesizing cubic-shaped zinc oxide). Characteristics of the reported MOF-177 have slight differences from each other, which might be caused by aberrations in the concentration and purity of the starting materials, also differences in heating and cooling rate. The relative characteristics of MOF-177 are Langmuir surface area of 4,170–5,640 m^2/g , BET surface area of 2,970–4,630 m^2/g , pore volume of 1.11–1.69 cm^3/g , and pore diameter 0.94–1.06 nm. The synthesized MOF-177 has a crystal clear appearance with a slightly yellow color and thermally stable in the air up to a temperature of 350°C [46].

Combination of terephthalic acid (1,4-benzenedicarboxylate, abbreviated as H_2BDC) and zinc nitrate as building blocks are used to synthesize MOF-5. The as-synthesized MOF-5 (also called as IRMOF-1) have a chemical composition of $Zn_4O(BDC)_3$ which have a three-dimensional cubic shape. MOF-5 is reportedly having a high surface area of 2,500 to 3,000 m^2/g owing to its scaffolding-like nature [46]. Both MOF-74 and IRMOF-3 have similar building blocks to that of MOF-5 but with the addition of functional groups in the organic linker structure. MOF-74 is synthesized from 2,5-dihydroxyterephthalic acid (H_4DOBDC) that has a similar structure to that of H_2BDC but with additional of two hydroxyl groups while in IRMOF-3, the functional group comes from its NH_2 - site.

Compared to that MOF-5, the addition of a functional group in the organic building block of IRMOF-3 and MOF-74 induce their reactivity towards VOCs. MOF-199 is another name given for MIL-100 (as discussed in section 12.4.1.3.), also refer to HKUST-1, is a copper-based MOF produced through a solvothermal reaction. While IRMOF-62 is synthesized from diacetylene-1,4-bis-(4-benzoic acid) and zinc acetate [46].

12.4.2.1 Adsorption Comparison of the Isorecticular MOFs

The adsorption capacity of the isorecticular MOFs is summarized in Table 12.5. Apparently, the adsorption capacity of the investigated MOFs not only depends on the surface area of MOFs, but also VOC type and reactivity, and the presence of MOF functional groups. The dependence of adsorption performance of MOFs toward the type of VOCs is apparent, in which a MOF might be effective in adsorbing one type of adsorbent but ineffective for other types of VOC. For instance, MOF-177 can adsorb ammonia 42-times higher than the other tested VOCs. Most of the investigated MOFs failed to adsorb chlorine; this is because chlorine cannot act as a ligand that binds to the metal cluster; unlike other VOCs. IRMOF-3 shows successful adsorption towards chlorine; this is ascribed to the reactive nature of the gas and also the effect of open metal sites as Lewis acids that interact with the adsorbate gases as Lewis base [46]. In the case of aromatic VOC (i.e., benzene), the adsorption may improve due to π - π interaction [29].

Based on Table 12.5, it is noted that a larger surface area not always in accordance with a higher adsorption capacity. MOF-177 and MOF-5 have larger BET surface area than other investigated MOFs, but they have the worst dynamic adsorption performance. MOFs with a large surface area may have a high capacity for thermodynamic adsorption; however, they are less effective in kinetic adsorption due to the absence of functional group that essential for the adsorbate-adsorbent interactions. The high surface area of IRMOF-62 seems to assist in enhancing the adsorption capacities; however, the lack of functional group caused IRMOF-62 to be less effective against certain VOC (i.e., sulfur dioxide) [46].

The role of MOF-functional groups in improving the adsorption performance can be noticed by comparing MOF-5, MOF-74, and IRMOF-3. Addition of NH_2 - functional group to the organic building block of MOF-5 produces IRMOF-3 which have better dynamic adsorption capacity; i.e., IRMOF-3 possesses adsorption capacity towards ammonia 18-times higher than MOF-5. Addition of OH- functional group (i.e., in producing MOF-74) also accentuate the adsorption performance. Such improvement

Table 12.5 Dynamic adsorption performance of some isoreticular MOFs against VOCs at gas flow 25 ml/min [46] and 600 ml/min [29].

Properties	MOF-177	MOF-5	MOF-74	IRMOF-3	MOF-199	IRMOF-62
BET surface area (m ² /g)	3,875	2,205	632	1,568	1,264	1,814
Adsorption capacity (mg/g) at gas flow rate of 25 ml/min						
Ammonia	42	6	93	105	87	23
Chlorine	<1	- ^a	- ^a	335	36	92
Tetrahydrothiophene	<1	1	90	7	351	84
Sulfur dioxide	<1	1	194	6	32	<1
Benzene	1	2	96	56	176	109
Dichloromethane	<1	<1	32	1	55	19
Ethylene oxide	<1	1	110	2	95	11
BET surface area (m ² /g)	2,970					
Adsorption capacity (mg/g) at gas flow rate of 600 ml/min						
Benzene	800					

^aExperiments not conducted due to apparatus corrosion by chlorine.

in adsorption capacity is due to the additional functional groups, such as amine, which function as electron rich groups that readily form hydrogen bonding with the adsorbate-molecules [46].

The vacant coordinated metal sites of MOF act as Lewis acids that is deficient of electron hence generate a stronger interaction with adsorbate molecules that can act as Lewis base, such as ammonia. The role of metal as Lewis acids can be observed in MOF-199 and MOF-74. Both MOF-199 and MOF-74 have open copper sites which can readily adsorb VOCs [46]. As presented in Table 12.5, apparently a larger gas purge flow may stimulate adsorption driving force thus promote penetration of VOC gas molecules into the porous matrix of the MOF. This insight can be drawn from adsorption capacity of MOF-177 at 600 ml/min gas flow which gave 800-times-higher benzene adsorption capacity compared to the studies done at 25 ml/min gas flow [29, 46].

12.4.3 NENU Series MOFs

A group in NENU (Northeast Normal University) synthesized another series of isorecticular MOF namely NENU-X. Prior to the synthesis of NENU-X MOFs, the organic linker used in a series of NENU MOFs was synthesized by integrating thiophene-containing bidentate ligand into benzene-1,3,5-tribenzoate (BTB). The MOFs were then synthesized through a solvothermal method with *N,N*-diethyl-formamide as a solvent (85°C, 2 days), and zinc nitrate was used as the metal source. The, as synthesized NENU-511 was built from coordination of six BTB to a six-connected node and possess meso- and micro-sized pore. Meanwhile, NENU-512, NENU-513, and NENU-514 have more disorderly structure due to their large-size pores [50].

The NENU-X MOFs have an enormous BET surface area up to 4240 m²/g, which play an important role in the adsorption of VOC, namely benzene. The adsorption capacity of the NENU-X MOFs against benzene is shown in Table 12.6. Adsorption of benzene onto NENU-511 and NENU-512, which do not possess a specific functional group on their inner matrix, is ascribed from their spacious matrix that can accommodate significant amount of benzene. Their spacious matrix also postponed their saturation to $P/P_0 = 0.20$. Meanwhile, NENU-513 and NENU-514 showed earlier saturation at $P/P_0 = 0.10$. This is due to the presence of phenyl-rings on the inner surfaces. While these phenyl-rings helps to enhance the adsorption towards benzene by raising the π - π interaction, excessive occurrence of phenyl-rings on the inner surface may reduce MOFs porosity and cause

Table 12.6 Surface area and adsorption capacity of NENU series toward benzene [50].

	NENU-511	NENU-512	NENU-513	NENU-514
Surface area (m ² /g)				
BET	4240	3648	3554	3457
Langmuir	6491	5640	5438	5320
Adsorption capacity (mg/g)	1556	1519	1687	1311

repulsion effect between each adsorbate molecules thus adversely affect adsorption capacity [50].

Another NENU-X MOF, namely NENU-520, has been synthesized by using a tetrazolate-containing ligand. However, no work has been done to study its adsorption ability against VOCs. Adsorption data of NENU-520 for CO₂ uptake has been reported by Lan *et al.*, where the uptake capacity is 79.9 cm³/cm³ at standard temperature and pressure [51].

12.4.4 MOF-5, Eu-MOF, and MOF-199

A research study by Vellingiri *et al.* demonstrated the superiority of MOF as adsorbent of VOC and semi-VOC, which is comparable to some commercial adsorbents (Tenax TA, Carboxen-1000, and Carboxen-1000) [28]. The adsorption ability of MOF-5, Eu-MOF, and MOF-199 against hydrocarbons, carboxylics, phenolics, and indoles VOC are investigated in their study. Some of the dynamic adsorption data from their research are shown in Table 12.7. MOF-199 show better adsorption performance compared to the other investigated MOFs; which was attributed from the effect of vacant copper-metal sites of MOF-199 that also act as Lewis sites. The lower adsorption capacities of Eu-MOF may be in consequence to the absence of vacant coordination sites and low adsorption energy of Eu metal. Meanwhile, the poor adsorption performance of MOF-5 is suggested to be the effect of its cubic-pore that eliminates the functionality of the frameworks.

Density functional theory (DFT) estimation revealed some specific interaction between the six-member ring compounds and MOFs that occurs during the adsorption of VOCs. The AA-stacking phenomena can be observed in the case of adsorption by using MOF-5, while higher

Table 12.7 The equilibrium adsorption capacity of MOF-5, Eu-MOF, and MOF-199 against several types of VOCs (selected from the Ref. [28]).

Properties	MOF		
	MOF-5	Eu-MOF	MOF-199
Surface area (m ² /g) ^a	535	281	1591
Pore volume (cm ³ /g)	0.22	0.95	0.46
SEM morphology	Cubic crystal	Grass-like crystal	Octahedral crystal
Adsorption capacity (mg/g)			
Aromatic VOCs mixture (p _i ^b)			
Benzene (8.6 mPa)	n. m. ^c	1.00	>1.1 ^d
Toluene (6.8 mPa)	n. m.	0.95	>2.6 ^d
<i>p</i> -Xylene (6.0 mPa)	n. m.	0.76	>5.2 ^d
Styrene (5.5 mPa)	n. m.	0.85	>4.9 ^d
Phenol VOCs mixture			
Phenol (12 mPa)	n. m.	1.50	13.0
<i>p</i> -Cresol (9.8 mPa)	1.50	3.00	15.0

^aLangmuir surface area; ^bpartial pressure of each species in VOCs mixture in parenthesis; ^cn.m. refers to not measurable; ^dsaturation of those adsorbates were not achieved within 15 L sample loading.

energy AB-stacking phenomena are observed for MOF-199. Moreover, the Cu-metal sites of MOF-199 can attract the compound containing polar –OH group thus increasing the adsorption capacity; this phenomenon does not occur in MOF-5 with Zn-ion as the central [28].

12.4.5 Amine-Impregnated MIL-100

MIL-100(Al) with amine functional group, coded as NH₂-MIL-101(Al) can be synthesized by reacting aluminum chloride salt with 2-amino terephthalic acid in DMF solvent (403K, 3days). The as synthesized NH₂-MIL-101 has BET surface area of 1943 m²/g. In static (liquid-phase) adsorption experiment, by using phenol and *p*-nitrophenol as adsorbate, NH₂-MIL-101(Al) can adsorb up to 1.2 mmol/g which is higher than some

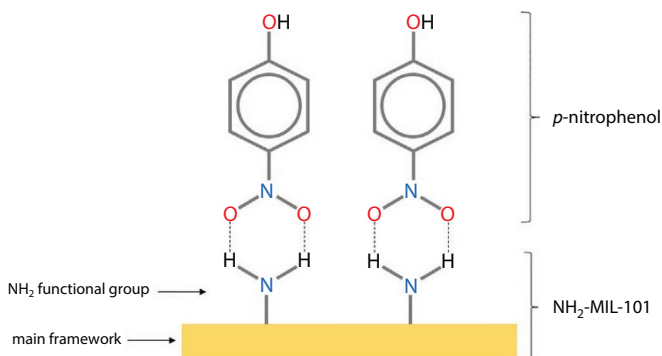


Figure 12.3 Adsorption of *p*-nitrophenol solution onto functionalized MOF. Amine group of NH_2 -MIL-101(Al) provides proton donor to the oxygen atoms of nitro group of *p*-nitrophenol. Redrawn from Ref. [27].

highly crosslinked-polymer such as HJ-1 (1.0 mmol/g) and Amberlite XAD (0.4 mmol/g). Hydrogen bonding plays an important role in promoting the adsorption of *p*-nitrophenol onto the amine-containing adsorbent as illustrated in Figure 12.3 [27].

12.4.6 Biodegradable MOFs MIL-88 Series

The sorption of nitric oxide (NO) onto a series of biocompatible and biodegradable Fe-based MOFs, namely MIL-88, has been studied. Various organic ligands, for instance fumarate-acetic acid, 1,4-benzenedicarboxylate (1,4-bdc), 2-nitroterephthalate (2- NO_2 -bdc), and 2,5-dihydroxyterephthalate (2,5-dhbd), have been used in the synthesized of MIL-88A, MIL-88B, MIL-88B- NO_2 , and MIL-88B-2OH, respectively. It is observed that the MIL-88 MOFs can adsorb a relatively low amount of NO approximately 1–2.5 mmol/g. The adsorption performance of MIL-88 series is affected by the accessibility of the gas penetration to the pore matrix which is quite low due to the absence of breathing ability; as a result, the gas cannot easily diffuse to interact with the central Fe metal cluster [52].

12.4.7 Catalytic MOFs

A certain metal cluster can produce MOFs with catalytic activity. A series of rare earth arenedisulfonate MOFs have been produced and tested for their catalytic activity. The tested MOFs are coded as LnPF-1 (Ln = La, Nd, Pr), LnPF-2 (Ln = Nd), and LnPF-3 (Ln = Nd) from the $\text{Ln}(\text{OH})(1,5\text{-NDS})\text{H}_2\text{O}$ (1,5-NDS = 1,5-naphthalenedisulfonate), $[\text{Ln}(\text{OH})(1,5\text{-NDS})$

$(\text{H}_2\text{O})_4$, and $\text{Ln}(\text{OH})_{4.5}(\text{2,6-NDS})_{1.5}(\text{H}_2\text{O})_2(\text{H}_2\text{O})$ (2,6-NDS = 2,6-naphthalenedisulfonate), respectively. LnPF-1, LnPF-2, and LnPF-3 showed catalytic activity in the conversion of linalool to produce cyclic hydroxyl ethers (furanoid and pyranoid) by H_2O_2 and MeCN at 70°C . The Ln-PF1 MOFs show the best catalytic activity with conversion yields (%) of 76, 94, and 100 (for Ln = Nd, Pr, and La, respectively) in relatively shorter reaction time (22-24 hours) compared to Ln-PF2 and LnPF-3 which barely can achieve 51% and 17% conversion after 48 h. The catalytic activity of the Ln-PF1, Ln-PF2, and Ln-PF3 induces by their metal clusters. There are eight neodymium (Nd) coordinations in Ln-PF1, and 9 Nd coordination in LnPF-2 and Ln-PF3; the high NdO_9 coordination in LnPF-2 and LnPF-3 makes it difficult for guest molecules to reach the active centers and thereby reducing the actuality of the catalyst. Better catalytic activity is shown by using praseodymium (Pr) and lanthanum (La) as the metal clusters in Ln-PF1, which is related to the decreasing of their radii [53].

Some other studied catalytic MOFs is the ytterbium (Yb) based MOFs, namely Yb-LRH with the cationic formula $[\text{Yb}_4(\text{OH})_{10}(\text{H}_2\text{O})_4]_n^{2+}$ and Yb-RPF-5 with formula $[\text{Yb}(\text{OH})(\text{2,6-AQDS})(\text{H}_2\text{O})]$ (AQDS = anthraquinone-2,6-disulfonate). The Yb-LRH is shown a selective-catalytic activity for the sulfide oxidation, while Yb-RPF-5 can catalyze hydrodesulfurization of thiophene (7 bar, 70°C) [54]. The use of Au as a metal cluster produced a MOF (Au@ZIF-8) that can catalyze the oxidation of carbon monoxide into CO_2 [55]. The $\text{NH}_4[\text{Cu}_3(\text{OH})(\text{capz})]$ -MOF, together with *t*-butyl hydroperoxide, show catalytic activity in the oxidation of cyclohexane and cyclohexene [56]. Also, it is worth to mention, a lot of molybdenum (Mo)-based MOFs show a catalytic behavior in the epoxidation of alkenes [57].

12.4.8 Photo-Degrading MOFs

Some MOFs possess adsorption and photo-degradation ability toward VOCs. The hybrid of TiO_2 nanoparticles within a typical NH_2 -UiO-66 MOF, namely $\text{TiO}_2@\text{NH}_2$ -UiO-66, have an excellent interface contact that allow the penetration of visible light and consequently accelerate the photogenerated electron-hole separation. The hybrid MOFs, which contain 5% TiO_2 , show a remarkable photo-degradation activity against styrene gas into CO_2 ; with removal efficiency >99% within 10 hours [58]. The Ti-Zr based MOFs, NH_2 -MIL-125 (TiZr15), shows a high photo-degradation activity of acetaminophen (with a pseudo-first order rate of 0.0121/min); the activity was found to be better compare to the bare Ti MOF. A better photo-degradation activity was achieved at lower Zr proportions. The

efficiency of photocatalytic activity of TiZr15 remains above 90% upon three successive acetaminophen conversion; which indicate its stability and reusability [59].

12.4.9 Some Other Studied MOFs

Various divalent metal ions have been used in the preparation of M-MOF-74 (where M = Zn, Co, Ni, Mg) and each metal produced MOF with different surface area, specifically 1206, 835, 599, 496 m²/g for M-MOF-74 with M = Mg, Co, Ni, Zn, respectively. The adsorptive ability of M-MOF-74 is tested against ammonia, cyanogen chloride, and sulfur dioxide. It is noted that the dynamic adsorption performance was different when conducted in dry and humid condition. As shown in Table 12.8, all MOF-74 analogs show better adsorption performance at dry condition. The adsorption capacity for all type of adsorbate was reduced when exposed to the humid gas stream; which suggests that there is a competition between the water molecules and adsorbate molecules to attach on the MOF surface [60].

Pyrazolate ligands and nickel hydroxo metal cluster have been used to synthesized some hydrophobic isorectulars MOFs, namely, [Ni₈(OH)₄(H₂O)₂(L)₆] or [Ni₈(L)₆]; where L symbolized various ligands such as H₂L1 (1H-pyrazole-4-carboxylic acid; H₂L2 (4-(1H-pyrazole-4-yl)benzoic acid), H₂L3 (4,4'-benzene-1,4-diylbis(1H-pyrazole)), H₂L4

Table 12.8 Dynamic adsorption data of MOF-74 analogues [60].

	Adsorption capacity (mmol/g)							
	Co-MOF-74		Mg-MOF-74		Ni-MOF-74		Zn-MOF-74	
	Dry	Wet	Dry	Wet	Dry	Wet	Dry	Wet
Ammonia	6.70	4.30	7.60	1.70	2.30	1.90	3.70	2.80
Cyanogen chloride	5.60	0.05	1.20	0.08	2.40	0.17	3.60	0.10
Sulfur dioxide	0.63	0.03	1.60	0.72	0.04	0.02	0.26	0.04
Amount of adsorbed water on adsorbent at different relative humidity (RH)								
15% RH	0.46		0.25		0.08		0.19	
50% RH	0.49		0.31		0.11		0.24	
80% RH	0.50		0.39		0.13		0.32	

(4,4'-buta-1,3-diyne-1,4-diylbis(1H-pyrazole)), H_2L5 (4,4'-(benzene-1,4-diyl)diethyne-2,1-diyl)bis(1H-pyrazole)), or H_2L5-R (R = methyl, trifluoromethyl). The geometry of the resulting MOFs is the combination of an octahedral and two tetrahedral cavities which analogues to that of UiO series MOFs. The BET surface area of the MOFs increases with the longer ligand chain; where the BET ranges between 205–2215 m^2/g with $[Ni_8(L1)_6]$ have the lowest BET (205 m^2/g), while $[Ni_8(L5)_6]$ have the largest BET (2215 m^2/g). The $[Ni_8(L)_6]$ series have been proven to be stable against hydrolysis with their bipyrazolate linkers are unaltered even after 24 h soaking in water. The hydrophobic nature of the $[Ni_8(L)_6]$ series allows performing adsorption under humid condition. Increase in hydrophobicity was observed by the presence of a fluorine functional group in $[Ni_8(L5-CF_3)_6]$. As reported, at 80% relative humidity, $[Ni_8(L5-CF_3)_6]$ is not suitable for water molecule adsorbent, in contrast to non-fluorine MOFs, e.g., $[Ni_8(L4)_6]$ and $[Ni_8(L5)_6]$ which possess high water adsorption capacity. The $[Ni_8(L5-CF_3)_6]$ show efficient adsorption against diethylsulfide under a very humid condition [61].

12.5 MOF Composites

12.5.1 MIL-101 Composite With Graphene Oxide

Combination of graphene oxide (GrO) with MIL-101 produced a composite (GrO@MIL-101) which suggest its potential in CO_2 and CH_4 removal. GrO@MIL-101 has the higher surface area and larger pore volume than that of MIL-101 prepared in the study; where the BET surface are (m^2/g), and pore volume (cm^3/g) for MIL-101 are 2670 and 1.28, while for GrO@MIL-101 are 2950 and 1.42. As revealed by SEM, the addition of GrO induced irregular particle shape of originally octahedral shaped MIL-101 [62]. The static adsorption study of the composite revealed that GrO@MIL-101 composite could remove CO_2 and CH_4 more effectively than MIL-101, as shown in Table 12.9. Also, at 1.5 bar, the adsorption selectivity of GrO@MIL-101 against CO_2/CH_4 was up to 32.

12.5.2 MIL-101 Composite With Graphite Oxide

Composites of MIL-101(Cr) and graphite oxide (GO), coded as MIL-101@GO- n , have been synthesized via the hydrothermal method by Sun *et al.* In their study, the composites were prepared by introducing n -amount of GO ($n = 2, 5, 10, \text{ and } 15 \text{ wt\%}$). As characterized by XRD, the addition of GO gives a reduction to the crystallinity of MIL-101(Cr). The SEM images

Table 12.9 Static adsorption performance of MIL-101 and its composite against CO₂ [62].

MOF composite	Adsorption model	Pressure (bar)	Adsorption capacity (mmol/g)		Desorption efficiency
			CO ₂	CH ₄	
MIL-101(Cr)	DSLFA	25	50.39	26.17	–
GrO@MIL-101(Cr)	DSLFA	25	66.12	37.21	>95%

^aDual Site Langmuir Freundlich (DSLFA) model equation.

revealed that the addition of GO causes the alteration of octahedral MIL-101(Cr) into irregular-shape particles. All of the composites possess a Type I isotherm-sorption as analyzed by N₂-sorption. The addition of GO also affecting the surface area of the prepared MOF-composites; where the BET surface area (m²/g) and pore volume (cm³/g, value in parenthesis) value are 2881.1 (1.36), 2988.6 (1.54), 3502.2 (1.75), 3318.6 (1.72), 1742.7 (1.00) for MIL-101, MIL-101@GO-2, MIL-101@GO-5, MIL-101@GO-10, and MIL-101@GO-15, respectively [63]. There is no certain decrementing or incrementing trend, caused by the addition of GO, observed for the surface area and pore volume. Reportedly, the addition of GO has been proven to increase the adsorption capacity toward *n*-hexane, as shown in Table 12.10. As shown in Table 12.10, MIL-101@GO-5 exhibit the highest adsorption of *n*-hexane compared to the other investigated MOF. The excellent adsorption performance of MIL-101@GO-5 is not only related to the high surface

Table 12.10 Static (vacuumed) adsorption performance of MIL-101 and its composite against *n*-hexane [63].

MOF composite	Adsorption model	Pressure (mbar)	Adsorption capacity (mg/g)	Desorption efficiency
MIL-101	L-FA	175	540.3	–
MIL-101@GO-5	L-FA	175	1042.1	–
MIL-101@GO-10	L-FA	175	952.8	96.78

^a Langmuir–Freundlich (L–F) model equation.

are but also due to the addition of GO in the proper ratio which in turns affect their surface dispersive force [63].

12.6 Generalization Adsorptive Removal of VOCs by MOFs

MOFs with the adsorptive surface that contain certain functional groups or vacant metal sites are more likely to have an enhanced adsorption efficiency toward adsorbate compounds. The organic building block of MOF which contain certain functional site can generate an electrostatic interaction or hydrogen bonding that can enhance their adsorption activity; meanwhile, vacant metal sites can promote coordination bond or π -interaction against the VOCs adsorbate. Adsorption transpires through continuous pore filling by VOCs to the inner and outer pore surfaces of the MOF. Pore filling by VOCs is possible since VOCs are vapors which have verge properties to non-ideal gases, with some deviations due to their gas-liquid phase equilibrium. The VOCs detention by MOF is consolidated through the non-covalent coupling involving the π -system of the metal cluster of MOF and VOCs. The π -interaction is triggered due to the different charge loading between the metal and VOCs. The metal cluster of MOF is an electron-poor system; meanwhile, the VOCs are the electron-rich system. The π -interaction is common, especially for the aromatic VOCs.

The adsorption of VOCs containing saturated chain, nonpolar property, and unbranched sites (e.g., hexane, heptane, and octane) are more likely occur due to physical interactions of the adsorbate molecules with the adsorbent lattice [64]. For aromatic molecules, a combination of physical and chemical adsorption may occur from the adsorbate and adsorbent interactions. Liu *et al.* demonstrated that the binding of benzene to the Lewis site of metal emerges due to the van der Waals and covalent bonding [65]. In adsorption of VOCs which behave as Lewis base (e.g., ammonia), the adsorption usually occurs as the effect of Lewis acid and Lewis base interaction. Ammonia molecules act as the Lewis base, while the metal sites serve as Lewis acid.

12.7 Simple Modeling the Adsorption

12.7.1 Thermodynamic Parameters

The Clausius–Clapeyron equation can be applied to estimate the heat of adsorption. The variation of retention volume (V_g) with the change of

temperature (T) can be translated into a mathematical equation to estimate the heat of adsorption ΔH_{ads} , Eq. (12.1) [61].

$$\Delta H_{\text{ads}} = -R \frac{\delta(\ln V_g)}{\delta(1/T)} \tag{12.1}$$

where R is the ideal gas constant. The V_g is directly related to Henry’s law constant (H_{lc}), the constant that stated the proportionality between the partial pressure of the gas phase to the quantity of gas dissolved [61]. In adsorption, the value of H_{lc} is directly related to that of the amount of gas adsorbed. The calculation of H_{lc} can be translated into a mathematical formula, as shown in Eq. (12.2).

$$H_{lc} = \frac{n_{\text{ads}}}{m \times P} \tag{12.2}$$

where, n_{ads} is the amount of gas adsorbed, m is the mass of adsorbent used, and p is the outlet pressure of gas.

A virial-type expansion, with virial coefficient A_i and B_p , also can be applied to estimate the heat of adsorption.

$$\ln P = \ln n_{\text{ads}} + \frac{1}{T} \sum_{i=0}^m A_i n_{\text{ads}}^i + \sum_{i=0}^n B_i n_{\text{ads}}^i \tag{12.3}$$

$$\Delta H_{\text{ads}} = -R \sum_{i=0}^m A_i n_{\text{ads}}^i \tag{12.4}$$

where m and n are the number of coefficients used to determine the isotherms [48].

12.7.2 Dynamic Sorption Methods

The determination of adsorption capacity of porous materials to adsorb gas adsorbate mostly done by using dynamic sorption methods since, in real practice, the gas adsorption is always done dynamically. Static volumetric measurements are one of (semi)-dynamic sorption methods in which the process conducts in a closed chamber, then the amount of gas adsorbed upon saturation at a given pressure (p / p_0) is recorded. The schematic diagram of the static volumetric and its resulting plot are shown in

Figure 12.4. The measurement only can be done for a single component, which is become the shortage of this method [66–69]. The amount of adsorbed gas can be calculated by treated the gas component as an ideal gas, as shown by the Eq. (12.5) below.

$$n_{\text{adsorbed}} = n_{\text{dosed}} - n_{\text{free}} = \left(\frac{pV}{RT} \right)_{\text{dose}} - (V_{\text{dose}} + V_{\text{chamber}}) \left(\frac{p}{RT} \right)_{\text{chamber}} \quad (12.5)$$

where n is the mol of gas, p is pressure, V is volume, T is temperature, and R is the ideal gas constant. The adsorption isotherm curve can be obtained by plotting amount of gas adsorbed vs. the given pressure.

A dynamic method proceeds under forced-flow conditions. The resulting data (that is adsorption time (duration of the test) vs. concentration of adsorbate in the effluent stream) is depicted as a breakthrough curve. The breakthrough curve (dynamic method) process is similar to that separation process in the industry, where the adsorbent is a gas mixture. The measurement itself is done in an open system while maintaining the pressure of the feed. The schematic diagram of the experimental setup and its corresponding breakthrough curve are depicted in Figure 12.5. Control of the gas flow rate is an important parameter that affected the amount of VOC introduced to the adsorption system, the acceleration of gas flow rate also directly related to the contact time between the VOC and MOF-adsorbent. The dynamic adsorption capacity can be calculated through breakthrough data by using the following series of equations [60, 66–69].

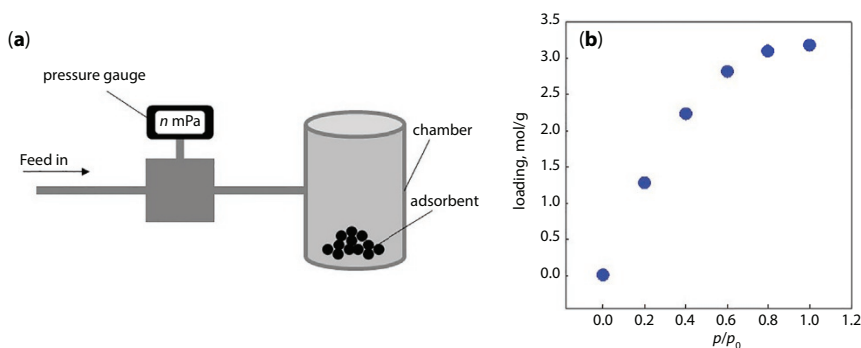


Figure 12.4 (a) Schematic diagram of static volumetric measurement; a single component of VOC gas is pressurized to the desired pressure and then introduced into a closed chamber filled with a certain amount of adsorbent. (b) Adsorption curve; obtained by plotting amount of gas adsorbed at saturation per given pressure.

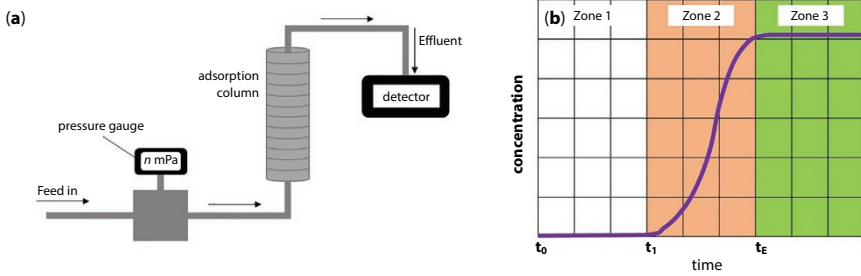


Figure 12.5 (a) Schematic diagram of dynamic method; the pressurized mixture of VOC gases continuously flowed into the adsorption column (filled with adsorbent) and the gas effluent is measured by using analytical device/detector. (b) Ideal S-shape breakthrough curve; zone 1—unsaturated zone, zone 2—mass transfer zone, zone 3—saturated zone.

The concentration of VOC over time (Ct , $\text{mg}\cdot\text{min}/\text{m}^3$) is calculated by multiply concentration of the feed (C_{feed} , mg/m^3) with the length of time that the feed passed (t_f , min), as shown in Eq. (12.6).

$$Ct_{\text{feed}} = t_f C_{\text{feed}} \tag{12.6}$$

The subsequent eluted concentration of VOC per time (Ct_{elution} , $\text{mg}\cdot\text{min}/\text{m}^3$) done by the adsorbent until the flow stopped can be calculated by integrating under the elution curve, as shown by Eq. (12.7); which also can be applied for desorption.

$$Ct_{\text{elution}} = \sum_{t=0}^{t_s} \frac{C_n + C_{n-1}}{2} \times (t_{n-1} - t_n) \tag{12.7}$$

in this case, t_s is saturation time (min), t_n is the time n (min), and C_n is the concentration at time n (mg/m^3) [60]. Note that there are many options of a modified form of the equations that can be used to modeling the adsorption experiment.

Zone 1, unsaturated zone, cannot be obtained by using the static volumetric measurements. Zone 2 is a mass transfer zone (also abbreviated as MTZ), the approximation of the effective-amount of adsorbent can be determined by analyzing the steepness of this zone. A very narrow zone 2 indicates that the adsorbent has a low adsorption capacity. The saturated zone, zone 3, is similar to that of the equilibrium value of adsorption isotherm in which the adsorption capacity can be determined. An ideal breakthrough curve would have an S-shaped curve, as shown in Figure 12.5.

An alteration (a skewed curve), however, may occur due to heterogeneity of the adsorbent [66–71].

12.8 Factor Affecting VOCs Adsorption

12.8.1 Breathing Phenomena

Breathing phenomena of MOF refers to the turnover structure from closed pores (non-porous) to open pores (porous). The phenomenon is pioneered by Ferey and Kitagawa *et al.* This dynamic phenomenon in adsorption is stimulated by atomic displacement (dipole moment interaction, in specific) which is caused by the presence of adsorbate. The phenomena are introduced by Kitagawa *et al.*, in their study on pillared layer MOFs. Kitagawa *et al.* declared that MOF is undergoing a locking and unlocking phenomena before and after adsorption, respectively [72, 73]. The distortion of the molecular structure of MOFs and cell-dimensions expansion occurred along with the breathing phenomena.

A similar breathing behavior observed for MIL-53. A reversible change in the pore volume happened when the MIL-53 (Al or Cr) is being air-cooled after heating at high temperature. As illustrated in Figure 12.6, a decrease in pore volume occurred when MIL-53 is at low temperature due to absorption of water molecules and reversed back to original volume when water molecules are removed by treating in high temperature. Upon high temperature treatment, the H-bond between the water molecules is getting weaker an

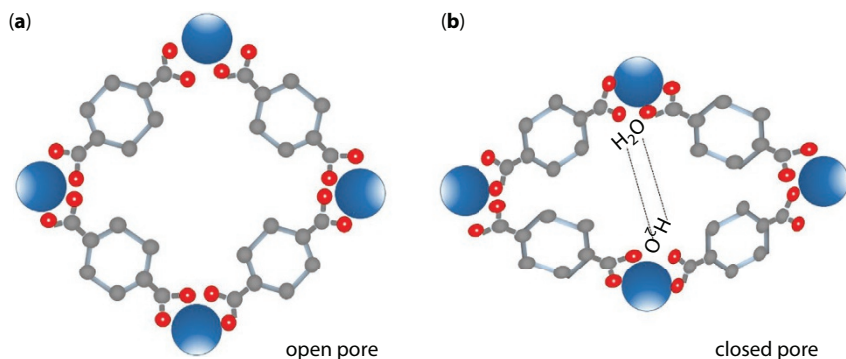


Figure 12.6 Illustrated breathing phenomena of MIL-53. (a) Open pore after high temperature treatment (unit cell volume 1522 Amstrong³); (b) closed pore (unit cell volume 1013 Amstrong³) after air cooling due to H-bond interactions between water molecules. Adapted from Ref. [74].

eventually disappeared along with the dehydration process; subsequently, the pores of MIL-53 convert back to large open pores [74].

A similar breathing phenomena also observed upon pressurized- CO_2 exposure to the hydrated MIL-53 at low temperature. CO_2 exposure at low pressure (<5 bar) is not sufficient to cause pore opening to MIL-53. The co-existence of open and closed pores is observed when the more CO_2 molecules are introduced, and consequently, the pressure is increased. Further increase of CO_2 pressure, > 15 bar (approximately 7.2 mmol/g), allow the presence of MIL-53 with the whole open pores. In this case, there is a slight different dehydrated phenomenon; that is, a two steps pore transition (open–closed–specific) is observed. Upon dehydration, a plateau (steady pore size) happens when 3.0 mmol/g CO_2 introduced. Hereafter, the pores start to expand as the CO_2 added (up to 7.7 mmol/g) before another plateau occurs. The plateau is suggested to be the effect of steric hindrance between the water molecules. The structural change due to the breathing effect also caused alteration to the sorption–isotherm behavior of MOFs. At dehydrated state, the N_2 -sorption of MIL-53 (both with Al or Cr building blocks) shows a Type-I-sorption-isotherm which indicate the dominance in microporous structure. A behavioral discrepancy is observed for MIL-53 with ferric (Fe) and scandium (Sc) metal center. Both dehydrated MIL-53(Fe) and (Sc) show nonporous structure; this difference is due to the two MOFs is initially have a closed or very-narrow pores unlike MIL-53(Al) or (Cr). When CO_2 introduced, instead of N_2 , a Type-VI-sorption-isotherm is observed. MOF attributed with breathing ability reportedly is chemically more stable than other MOFs without this ability. MIL-53, for instance, remains indestructible either in the presence of water molecules or heat up to 500°C [44, 75, 76].

12.8.2 Activation of MOFs

Many studies reported that the enormous surface area and porosity of MOFs can be achieved by removing the guest molecules from the framework matrix without destroying the integrity of the structure and pores [77]. This process is called activation or sometimes referred to as purification. The presence of guest molecules is originated by the excess reactant, solvent, and reaction intermediate ion or molecules. Often, those guest molecules cause pore blocking, thus reducing the surface area as well as pore volume of MOFs; subsequently, they may also demote the adsorption performance of MOFs. For instance, the presence of dimethylformamide (DMF) residual-guest molecules in the structural of BioMIL-3

([Ca₂(azbz-TC)-(H₂O)(DMF)], azbz-TC = 3,3',5,5'-azobenzene tetracarboxylate) cause steric hindrance and diffusion blocking thus constraint the interaction of the gas adsorbate (nitric oxide) with the metal sites [78]. In some cases, activation of MOFs may also grant breathing ability to MOFs [79]. Several activation processes have been developed by engineers, such as heat treatment, vacuum treatment, chemical treatment, solvent exchange, supercritical treatment, and freeze drying.

Ideally activation process by using heat treatment can only be successfully applied to MOFs with high thermal stability. However, in most cases, the implementation of heat activation fails to purify the pore and may destruct the crystallinity of the MOFs in response to the demolition of the coordination bond of MOFs by a large amount of heat energy. A subclass of MOFs namely ZIF-8 (ZIF = zeolitic imidazolate framework) with surface area 874 m²/g show an improvement in adsorption activity upon heat treatment. The adsorption capacity of ZIF-8 towards toluene increased from 5.4 to 41.1 mg/g after heating treatment at 300°C [80]. Similarly, vacuum treatment is also known to cause loss of crystallinity due to the large capillary forces and surface tension (as the liquid phase transforms into gas phase) that result in the destruction of MOF coordination bonds. In chemical treatment, a strong acid solution is commonly used to rigorously wash the guest molecules out of the pore of MOF. Activation by the solvent is done by exchanging the high boiling point solvent with a lower boiling point solvent, this is to minimize the molecular forces caused by the solvent during activation. Supercritical treatment is basically similar to that solvent exchange, but the treatment is done at supercritical condition by using liquid CO₂ as the common solvent. The implementation of freeze drying activation is preceded by the introduction of benzene into MOFs followed by several freezing-thawing cycles [77, 81–84].

12.8.3 Applied Pressure

Application of pressure play an important role in promoting the adsorbate-adsorbent interaction. Hamon *et al.* show that adsorption of H₂S onto MIL-53(Cr) at low pressure (4.5 kPa) resulting in low adsorption capacity of 3.02 mmol/g. At higher applied pressure of 1.6 MPa, 13.12 mmol H₂S can be adsorbed per gram of MIL-53(Cr). This behavior attributed to the breathing of MIL-53(Cr). At low pressure, closing pore phenomena occurs due to the strong interaction of OH-group of MOF with H₂S. At higher pressure, there is a complete pore vacancy as the interaction of OH-group of MOF with H₂S getting weaker. The pore opening is allowing the total filling of the pores, which leads to higher adsorption capacity [38].

12.8.4 Relative Humidity

Adsorption which performed in humid gas flow or in the presence of water molecules, may have a decreased adsorption capacity. As shown in Table 12.5, the adsorption performs in a dry gas flow have better adsorption capacities than that of wet flow. A similar phenomenon also occurs in the adsorption study of MOF-177 by Yang *et al.* The adsorption of toluene and trichloroethylene on MOF-177 is decreased steeply as the relative humidity altered from 0% to 50%. The water molecules initiate competition against adsorbate to bind to the open metal sites of MOF, thus cause suppressions to the adsorption performance. The other possibility is that the exposure of water to MOF may disrupt its structure [29, 60]. In particular, [Ni(bpb)] MOF may effectively adsorb VOCs in a humid condition. In a dynamic adsorption experiment with 60% humidity, 1 g of [Ni(bpb)] (which synthesized from organic linker namely 1,4-(4-bispyrazolyl)benzene (bpb)) can adsorb 340 mg of thiopene [85].

12.8.5 Breakthrough Conditions

As so called breakthrough curve give a full depiction of adsorption dynamic. The curve shows the change of VOC concentration in the effluent throughout adsorption time. The sorption capacity, thermodynamic (heat transfer or release), kinetics (adsorption rate), selectivity, and gas flow rate are the crucial parameters that influence the curve. An adsorbent with large sorption capacity will have longer breakthrough times since it can retain more adsorbate molecules. However, if the sorption kinetics proceed very slowly, there is a possibility of the spontaneous breakthrough, this will cause alteration in the shape of the curve. A rapid mass transfer (high flow rate) produces a steep breakthrough curve and narrow mass transfer zone. Broadening of the mass transfer zone may occur in the case of exothermic adsorption. The temperature increase due to heat release by adsorption leads to flatter and more asymmetric curve. An evenly mass dispersion may also lead to broadening of the mass transfer zone [69].

12.8.6 Functional Group of MOFs

The presence of functional groups of MOF in enhancing the adsorption has been demonstrated. A particular functional group may also help to prevent competition between adsorbate molecules and water molecules; consequently, the adsorption still performs excellently in the humid condition. Addition of fluorine in the building block of FMOF-1 (prepared by reacting

monovalent silver and 3,5-bis(trifluoromethyl)-1,2,4-triazolate) cause it to be hydrophobic, therefore the water molecules cannot enter the pore of FMOF-1. The hydrophobicity of FMOF-1 also makes it be selective against certain VOCs (benzene, *p*-xylene, cyclohexane, toluene, and *n*-hexane) [86]. A similar phenomenon is observed for $[\text{Ni}_8(\text{OH})_4(\text{H}_2\text{O})_2(\text{L5-CF}_3)_6]$, which build from 4,4'-(benzene-1,4-diyl)diethyne-2,1-diyl)bis(1*H*-pyrazole) abbreviated as L5. The presence of coordination of the metal with the pyrazole group induces the stability of the MOF against water molecules, and the MOF still able to adsorb diethylsulfide at 80% relative humidity [61].

The presence of the ionic group in the MOF structure may induce selectivity against certain VOC. The NH_4^+ in the framework of MOF namely $\text{NH}_4[\text{Cu}_3(\text{OH})(\text{capz})]$, where capz = 4-carboxypyrazolato, causes alteration in the pore structure of the MOF and also lead to adsorption selectivity toward cyclohexane-benzene mixtures, which related to the size-exclusion of the adsorbate molecules.

12.8.7 Concentration, Molecular Size, and Type of VOCs

Adsorption can occur effectively when there is compatibility between VOCs and MOFs as the guest and host molecules. The key features of the compatibility, in this case, are the molecular size, molecular orientation, and the number of molecules of the VOC adsorbate. Adsorption can occur efficiently when all key features of VOCs are consistent with the pore structure and crystal symmetry of MOF as adsorbent. For instance, MIL-53(Al) can adsorb doubled amount of *p*-xylene when the pore is in the vacant form. The availability of space in the vacant pore is adequate to accommodate two molecules of *p*-xylene as illustrated in Figure 12.7. Also, the length of *p*-xylene is compatible with the size of MIL-53 open pore [75]. If the amount of adsorbate molecules is too many, the active adsorption sites of the adsorbent may not enough to accommodate all of the desired adsorbate molecules (saturation of the adsorbent). Also, there might be repulsive force between the adsorbate molecules thus decrease the efficiency of the adsorption.

The type of VOC adsorbents determines the adsorption performance. The strength of inter- or intra-molecular interaction of each type of VOC is determined by their affinity; the interaction can be polarization and/or electrostatic, acid-base, or physisorption. A density functional theory has been applied to investigate the adsorption energies between several small organic molecules with a copper metal cluster of HKUST-1. It is revealed that only the adsorption energy of NH_3 can surpass the

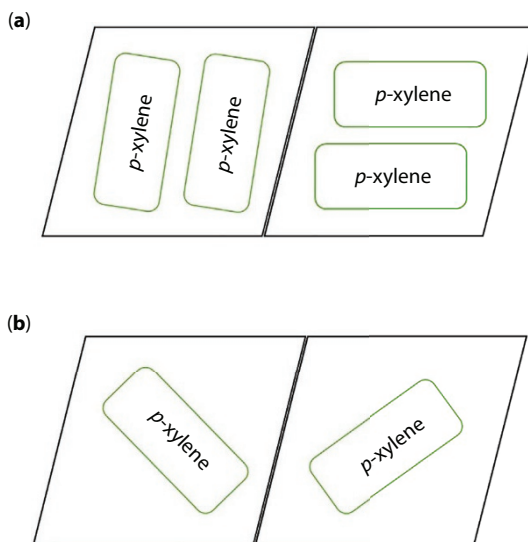


Figure 12.7 Adsorption of *p*-xylene by MIL-53 at open pore condition. (a) There is double amount of *p*-xylene adsorbed when the molecular orientation is compatible with pore structure and symmetry, (b) a lesser amount of *p*-xylene can be adsorbed since the orientation is not compatible. Adapted from Ref. [75].

water molecules; with the value of adsorption energies is decreased in the following order: $\text{NH}_3 > \text{H}_2\text{O} > \text{PH}_3 > \text{H}_2\text{S} > \text{SO}_2 > \text{CO} \sim \text{OCS} \sim \text{CO}_2 \sim \text{N}_y\text{O}_x > \text{N}_2 > \text{O}_2$ [87].

12.9 Future Perspective

The superiority and efficacy of MOF in overcoming VOCs has been proven by many engineers. MOF can be used as an efficient adsorbent for removing and/or storing VOCs, some MOFs also have catalytic activity against VOCs. In many lab scale experiments, it has been shown that the MOF adsorption capacity is very high; i.e., can reach >1 g VOC per g MOF. But there are still very few experiments that show the feasibility of VOC adsorption by MOF on an industrial scale. The feasibility of MOF application in the industry can be said to be far from ideal, both in terms of economics and synthesis. This is because in industry, VOC is always produced in large quantities so it requires large amounts of MOF as an adsorbent; this will cause an increase in total production costs due to the high cost of MOF synthesis.

References

1. Barea, E., Montoro, C. *et al.*, Toxic gas removal – metal–organic frameworks for the capture and degradation of toxic gases and vapours. *Chem. Soc. Rev.*, 43, 5419, 2014.
2. Wen, M., Li, G. *et al.*, Metal–organic framework-based nanomaterials for adsorption and photocatalytic degradation of gaseous pollutants: Recent progress and challenges. *Environ. Sci. Nano*, 6, 1006, 2019.
3. United States Environmental Protection Agency, 2017. Technical Overview of Volatile Organic Compounds, <https://www.epa.gov/indoor-air-quality-iaq/technical-overview-volatile-organic-compounds>.
4. Shuai, J., Kim, S. *et al.*, Health risk assessment of volatile organic compounds exposure near Daegu dyeing industrial complex in South Korea. *BMC Public Health*, 18, 528, 2018.
5. Lin, L., Chai, Y. *et al.*, Photocatalytic oxidation for degradation of VOCs. *Open J. Inorg. Chem.*, 3, 14–25, 2013.
6. Khan, F.I. and Ghosal, A.K., Removal of Volatile Organic Compounds from polluted air. *J. Loss Prevent. Proc.*, 13, 527–545, 2000.
7. U.S. National Library of Medicine, 2017. Volatile Organic Compounds (VOCs), <https://toxtown.nlm.nih.gov/chemicals-and-contaminants/volatile-organic-compounds-vocs>.
8. The National Institute for Occupational Safety and Health (NIOSH), Centers for Disease Control and Prevention, The NIOSH Pocket Guide to Chemical Hazards, <https://www.cdc.gov/niosh/npg/pgintrod.html>.
9. Loreto, F. and Fares, S., Biogenic Volatile Organic Compounds and Their Impacts on Biosphere–Atmosphere Interactions, in: *Developments in Environmental Science*, Matyssek, R., *et al.* (Eds.), pp. 57–75.
10. Peñuelas, J., Asensio, D. *et al.*, Biogenic volatile emissions from the soil. *Plant Cell Environ.*, 37, 1866–1891, 2014.
11. Ryu, C.-M., Farag, M.A. *et al.*, Bacterial volatiles promote growth in *Arabidopsis*. *PNAS*, 100, 4927–4932, 2003.
12. Naznin, H.A., Kiyohara, D. *et al.*, Systemic Resistance Induced by Volatile Organic Compounds Emitted by Plant Growth-Promoting Fungi in *Arabidopsis thaliana*. *PLoS One*, 9, e86882, 2014.
13. Jaeger, D.M., Runyon, J.B. *et al.*, Signals of speciation: Volatile organic compounds resolve closely related sagebrush taxa, suggesting their importance in evolution. *New Phytol.*, 211, 1393–1401, 2016.
14. González-Mas, M.C., Rambla, J.L. *et al.*, Volatile Compounds in *Citrus* Essential Oils: A Comprehensive Review. *Front. Plant Sci.*, 10, 12, 2019.
15. Shao, M., Czapiewski, K.V. *et al.*, Volatile organic compound emissions from Scot pine: Mechanisms and description by algorithms. *J. Geophys. Res.*, 106, 20483–20491, 2001.
16. Rasmann, S., Köllner, T.G. *et al.*, Recruitment of entomopathogenic nematodes by insect-damaged maize roots. *Nature*, 434, 732–737, 2005.

17. Fialho, M.B., Toffano, L. *et al.*, Volatile organic compounds produced by *Saccharomyces cerevisiae* inhibit the *in vitro* development of *Guignardia citricarpa*, the causal agent of citrus black spot. *World J. Microbiol. Biotechnol.*, 26, 925–932, 2010.
18. Oro, L., Feliziani, E. *et al.*, Volatile organic compounds from *Wickerhamomyces anomalus*, *Metschnikowia pulcherrima* and *Saccharomyces cerevisiae* inhibit growth of decay causing fungi and control postharvest diseases of strawberries. *Int. J. Food Microbiol.*, 265, 18–22, 2018.
19. Cuffia, F., Bergamini, C.V. *et al.*, Characterization of volatile compounds produced by *Lactobacillus helveticus* strains in a hard cheese model. *Food Sci. Technol. Int.*, 24, 67–77, 2017.
20. Chen, J., Tang, J.N. *et al.*, The production characteristics of volatile organic compounds and their relation to growth status of *Staphylococcus aureus* in milk environment. *J. Dairy Sci.*, 101, 4983–4991, 2018.
21. Ezeji, T.C., Qureshi, N. *et al.*, Production of acetone, butanol and ethanol by *Clostridium beijerinckii* BA101 and *in situ* recovery by gas stripping. *World J. Microbiol. Biotechnol.*, 19, 595–603, 2003.
22. Daisy, B.H., Strobel, G.A. *et al.*, Naphthalene, an insect repellent, is produced by *Muscodora vitigenus*, a novel endophytic fungus. *Microbiology*, 148, 3737–3741, 2002.
23. Singh, S.K., Strobel, G.A. *et al.*, An endophytic *Phomopsis* sp. possessing bioactivity and fuel potential with its volatile organic compounds. *Microb. Ecol.*, 61, 729–739, 2011.
24. G. Strobel, D. Manker *et al.*, Endophytic fungi and methods of use. U.S. Patent 7754203, assigned to Agra Quest, Inc. 2010.
25. Drilling, K. and Dettner, K., Electrophysiological responses of four fungivorous coleoptera to volatiles of *Trametes versicolor*: Implications for host selection. *Chemoecology*, 19, 109–115, 2009.
26. Hussain, A., Tian, M.Y. *et al.*, Differential fluctuation in virulence and VOC profiles among different cultures of entomopathogenic fungi. *J. Invertebr. Pathol.*, 104, 166–171, 2010.
27. Liu, B., Yang, F. *et al.*, Adsorption of Phenol and *p*Nitrophenol from Aqueous Solutions on Metal–Organic Frameworks: Effect of Hydrogen Bonding. *J. Chem. Eng. Data*, 59, 1476–1482, 2014.
28. Vellingiri, K., Szulejko, J.E. *et al.*, Metal organic frameworks as sorption media for volatile and semi-volatile organic compounds at ambient conditions. *Sci. Rep.*, 6, 27813, 2016.
29. Yang, K., Xue, F. *et al.*, Adsorption of volatile organic compounds by metal–organic frameworks MOF-177. *J. Environ. Chem. Eng.*, 1, 713–718, 2013.
30. Zhang, G., Liu, Y. *et al.*, Adsorption of volatile organic compounds onto natural porous minerals. *J. Hazard. Mater.*, 364, 317–324, 2019.
31. Yang, H., Deng, J. *et al.*, Au/MnOx/3DOM SiO₂: Highly active catalysts for toluene oxidation. *Appl. Catal., A*, 507, 139–148, 2015.

32. Hao, X., Li, R. *et al.*, Numerical simulation of a regenerative thermal oxidizer for volatile organic compounds treatment *Environ. Eng. Res.*, 2018.
33. Christen, P., Domenech, F. *et al.*, Biofiltration of volatile ethanol using sugar cane bagasse inoculated with *Candida utilis*. *J. Hazard. Mater.*, 89, 253–265, 2002.
34. Lalanne, F., Malhautier, L. *et al.*, Absorption of a mixture of volatile organic compounds (VOCs) in aqueous solutions of soluble cutting oil. *Bioresour. Technol.*, 99, 1699–1707, 2008.
35. Rebollar-Perez, G., Carretier, E. *et al.*, Volatile Organic Compound (VOC) Removal by Vapor Permeation at Low VOC Concentrations: Laboratory Scale Results and Modeling for Scale Up. *Membranes*, 1, 80–90, 2011.
36. Alivand, M.S., Shafiei-Alavijeh, M. *et al.*, Facile and high-yield synthesis of improved MIL-101(Cr) metal–organic framework with exceptional CO₂ and H₂S uptake; the impact of excess ligand-cluster. *Microporous Mesoporous Mater.*, 279, 153–164, 2019.
37. Du, P.D., Thanh, H.T.M. *et al.*, Metal–Organic Framework MIL-101: Synthesis and Photocatalytic Degradation of Remazol Black B Dye. *J. Nanomat.*, 2019, Article ID 6061275, 15 pages, 2019.
38. Hamon, L., Serre, C. *et al.*, Comparative Study of Hydrogen Sulfide Adsorption in the MIL-53(Al, Cr, Fe), MIL-47(V), MIL-100(Cr), and MIL-101(Cr) Metal–Organic Frameworks at Room Temperature. *J. Am. Chem. Soc.*, 131, 8775–8777, 2009.
39. Huang, C.-Y., Song, M. *et al.*, Probing the Adsorption Characteristic of Metal–Organic Framework MIL-101 for Volatile Organic Compounds by Quartz Crystal Microbalance. *Environ. Sci. Technol.*, 45, 4490–4496, 2011.
40. Leng, K., Sun, Y. *et al.*, Rapid Synthesis of Metal–Organic Frameworks MIL-101(Cr) Without the Addition of Solvent and Hydrofluoric Acid. *Cryst. Growth Des.*, 16, 1168–1171, 2016.
41. Shafiei, M., Alivand, M.S. *et al.*, Synthesis and adsorption performance of a modified micro-mesoporous MIL-101(Cr) for VOCs removal at ambient conditions. *Chem. Eng. J.*, 341, 164–174, 2018.
42. Yot, P.G., Ma, Q. *et al.*, Large breathing of the MOF MIL-47(V^{IV}) under mechanical pressure: A joint experimental–modelling exploration. *Chem. Sci.*, 3, 1100–1104, 2012.
43. Boutin, A., Coudert, F.-X. *et al.*, The Behavior of Flexible MIL-53(Al) upon CH₄ and CO₂ Adsorption. *J. Phys. Chem. C*, 114, 22237–22244, 2010.
44. Alhamami, M., Doan, H. *et al.*, A Review on Breathing Behaviors of Metal–Organic-Frameworks (MOFs) for Gas Adsorption. *Materials*, 7, 3198–3250, 2014.
45. Finsy, V., Kirschhock, C.E. *et al.*, Framework breathing in the vapour-phase adsorption and separation of xylene isomers with the metal–organic framework MIL-53. *Chemistry*, 15, 7724–7731, 2009.

46. Britt, D., Tranchemontagne, D. *et al.*, Metal–organic frameworks with high capacity and selectivity for harmful gases. *Proc. Natl. Acad. Sci.*, 105, 11623–11627, 2008.
47. Chae, H.K., Siberio-Pérez, D.Y. *et al.*, A route to high surface area, porosity and inclusion of large molecules in crystals. *Let. Nature*, 427, 523–527, 2004.
48. Furukawa, H., Miller, M.A. *et al.*, Independent verification of the saturation hydrogen uptake in MOF-177 and establishment of a benchmark for hydrogen adsorption in metal–organic frameworks. *J. Mater. Chem.*, 17, 3197–3204, 2007.
49. Tranchemontagne, D.J., Hunt, J.R. *et al.*, Room temperature synthesis of metal–organic frameworks: MOF-5, MOF-74, MOF-177, MOF-199, and IRMOF-0. *Tetrahedron*, 64, 8553–8567, 2008.
50. He, W.-W., Yang, G.-S. *et al.*, Phenyl Groups Result in the Highest Benzene Storage and Most Efficient Desulfurization in a Series of Isostructural Metal–Organic Frameworks. *Chem. Eur. J.*, 21, 9784–9789, 2015.
51. Bao, S.-J., Krishna, R. *et al.*, A stable metal–organic framework with suitable pore sizes and rich uncoordinated nitrogen atoms on the internal surface of microspores for highly efficient CO₂ capture. *J. Mater. Chem. A*, 3, 7361–7367, 2015.
52. McKinlay, A.C., Eubank, J.F. *et al.*, Nitric Oxide Adsorption and Delivery in Flexible MIL-88(Fe) Metal–Organic Frameworks. *Chem. Mater.*, 25, 1592–1599, 2013.
53. Gándara, F., García-Cortés, A. *et al.*, Rare Earth Arenedisulfonate Metal–Organic Frameworks: An Approach toward Polyhedral Diversity and Variety of Functional Compounds. *Inorg. Chem.*, 46, 3475–3484, 2007.
54. Gándara, F., Puebla, E.G. *et al.*, Controlling the Structure of Arenedisulfonates toward Catalytically Active Materials. *Chem. Mater.*, 21, 655–661, 2009.
55. Jiang, H.L., Liu, B. *et al.*, Au@ZIF-8: CO oxidation over gold nanoparticles deposited to metal–organic framework. *J. Am. Chem. Soc.*, 131, 11302–11303, 2009.
56. Procopio, E.Q., Linares, F. *et al.*, Cation-Exchange Porosity Tuning in Anionic Metal–Organic Frameworks for the Selective Separation of Gases and Vapors and for Catalysis. *Angew. Chem. Int. Ed.*, 49, 7308, 2010.
57. Shen, Y., Jiang, P. *et al.*, Recent Progress in Application of Molybdenum-Based Catalysts for Epoxidation of Alkenes. *Catalysts*, 9, 31, 2019.
58. Yao, P., Liu, H. *et al.*, Enhanced visible-light photocatalytic activity to volatile organic compounds degradation and deactivation resistance mechanism of titania confined inside a metal–organic framework. *J. Colloid Interface Sci.*, 522, 174–182, 2018.
59. Gómez-Avilés, A., Peñas-Garzón, M. *et al.*, Mixed Ti–Zr metal–organic frameworks for the photodegradation of acetaminophen under solar irradiation. *Appl. Catal., B*, 253, 253–262, 2019.
60. Glover, T.G., Peterson, G.W. *et al.*, MOF-74 building unit has a direct impact on toxic gas adsorption. *Chem. Eng. Sci.*, 66, 163–170, 2011.

61. Padial, N.M., Procopio, E.Q. *et al.*, Highly Hydrophobic Isoreticular Porous Metal–Organic Frameworks for the Capture of Harmful Volatile Organic Compounds. *Angew. Chem. Int. Ed.*, 52, 1–6, 2013.
62. Zhou, X., Huang, W. *et al.*, Enhanced separation performance of a novel composite material GrO@MIL-101 for CO₂/CH₄ binary mixture. *Chem. Eng. J.*, 266, 339–344, 2015.
63. Sun, X., Xia, Q. *et al.*, Synthesis and adsorption performance of MIL-101(Cr)/graphite oxide composites with high capacities of n-hexane. *Chem. Eng. J.*, 239, 226–232, 2014.
64. Hercigonja, R. and Rakić, V., Enthalpy–entropy Compensation for n-hexane Adsorption on Y Zeolite Containing Transition Metal Cations. *Sci. Sinter.*, 47, 83–88, 2015.
65. Liu, W., Carrasco, J. *et al.*, Benzene Adsorbed on Metals: Concerted Effect of Covalency and van der Waals Bonding. *Phys. Rev. B*, 86, 245405, 2012.
66. Möller, A., Eschrich, R. *et al.*, Dynamic and equilibrium-based investigations of CO₂-removal from CH₄-rich gas mixtures on microporous adsorbents. *Adsorption*, 23, 197–209, 2017.
67. Grande, C.A., Blom, R. *et al.*, High-Pressure Separation of CH₄/CO₂ Using Activated Carbon. *Chem. Eng. Sci.*, 89, 10–20, 2013.
68. Bastos-Neto, M., Moeller, A. *et al.*, Adsorption Measurements of Nitrogen and Methane in Hydrogen-Rich Mixtures at High Pressures. *Ind. Eng. Chem. Res.*, 50, 10211–10221, 2011.
69. INSTRUMENTS GmbH & Co. KG, 2019. Dynamic Sorption, <https://www.dynamicsorption.com/dynamic-sorption-method/breakthrough-measurement/>.
70. Hori, H., Tanaka, I. *et al.*, Breakthrough Time on Activated Carbon Fluidized Bed Adsorbers. *J. Air Pollut. Control Assoc.*, 38, 269–271, 1988.
71. Wang, W.-Z., Brusseau, M.L. *et al.*, Nonequilibrium and Nonlinear Sorption during Transport of Cadmium, Nickel, and Strontium through Subsurface Soils. *Adsorpt. Met. Geomedia*, 427–443, 1998.
72. Kitagawa, S., Kitaura, R. *et al.*, Functional Porous Coordination Polymers. *Angew. Chem. Int. Ed.*, 43, 2334, 2004.
73. Foo, M.L., Matsuda, R. *et al.*, An Adsorbate Discriminatory Gate Effect in a Flexible Porous Coordination Polymer for Selective Adsorption of CO₂ over C₂H₂. *J. Am. Chem. Soc.*, 138, 3022–3030, 2016.
74. Serre, C., Millange, F. *et al.*, Very Large Breathing Effect in the First Nanoporous Chromium(III)-Based Solids: MIL-53 or Cr^{III}(OH)·{O₂C–C₆H₄–CO₂}·{HO₂C–C₆H₄–CO₂H}_x·H₂O_y. *J. Am. Chem. Soc.*, 124, 13519–13526, 2002.
75. Wu, H., Gong, Q. *et al.*, Commensurate adsorption of hydrocarbons and alcohols in microporous metal organic frameworks. *Chem. Rev.*, 112, 836–868, 2012.

76. Llewellyn, P.L., Bourrelly, S. *et al.*, How hydration drastically improves adsorption selectivity for CO₂ over CH₄ in the flexible chromium terephthalate MIL-53. *Angew. Chem. Int. Ed.*, 45, 7751–7754, 2006.
77. Mondloch, J.E., Karagiari, O. *et al.*, Activation of metal–organic framework materials. *Cryst. Eng. Comm.*, 15, 9258–9264, 2013.
78. Miller, S.R., Alvarez, E. *et al.*, A rare example of a porous Ca-MOF for the controlled release of biologically active NO. *Chem. Commun.*, 49, 7773, 2013.
79. Engel, E.R., Jouaiti, A. *et al.*, Activation-Dependent Breathing in a Flexible Metal–Organic Framework and the Effects of Repeated Sorption/Desorption Cycling. *Angew. Chem. Int. Ed.*, 56, 8874–8878, 2017.
80. Jafaria, S., Ghorbani, F. *et al.*, Removal of Toluene from Air by Zeolitic Imidazolate Framework-8: Synthesis, Characterization, and Experimental Breakthrough Curve. *Int. J. Sci. Stud.*, 5, 1073–1082, 2017.
81. Abraham, B.F., Hoskins, B.F. *et al.*, Assembly of porphyrin building blocks into network structures with large channels. *Nature*, 369, 727–729, 1994.
82. Bedia, J., Muelas-Ramos, V. *et al.*, A Review on the Synthesis and Characterization of Metal Organic Frameworks for Photocatalytic Water Purification. *Catalysts*, 9, 52, 2019.
83. Férey, G., Mellot-Draznieks, C. *et al.*, A chromium terephthalate-based solid with unusually large pore volumes and surface area. *Science*, 23, 2040–2042, 2005.
84. Cavka, J.H., Jakobsen, S. *et al.*, A new zirconium inorganic building brick forming metal organic frameworks with exceptional stability. *J. Am. Chem. Soc.*, 130, 13850–13851, 2008.
85. Galli, S., Masciocchi, N. *et al.*, Adsorption of Harmful Organic Vapors by Flexible Hydrophobic Bis-pyrazolate Based MOFs. *Chem. Mater.*, 22, 1664–1672, 2010.
86. Yang, C., Kaipa, U. *et al.*, Fluorous metal–organic frameworks with superior adsorption and hydrophobic properties toward oil spill cleanup and hydrocarbon storage. *J. Am. Chem. Soc.*, 133, 18094–18097, 2011.
87. Supronowicz, B., Mavrandonakis, A. *et al.*, Interaction of Small Gases with the Unsaturated Metal Centers of the HKUST-1 Metal Organic Framework. *J. Phys. Chem. C*, 117, 14570–14578, 2013.